DELPHI Collaboration

DELPHI 2004-012-CONF-688
8 July, 2004

Updated DELPHI results on neutral Higgs bosons in MSSM benchmark scenarios

V. Ruhlmann-Kleider
CEA, DSM/DAPNIA/SPP, Saclay

Abstract

This note presents the interpretation of the results obtained by DELPHI at both LEP1 and LEP2 on the searches for MSSM neutral Higgs bosons, in the framework of a few benchmark scenarios. The interpretation is based on the same experimental inputs as the note submitted one year ago at the summer conferences on a similar subject, but uses updated theoretical calculations with more complete two-loop order radiative corrections. Limits on the h and A masses and on $\tan\beta$ are derived and their dependence on the top quark mass is presented.

Contributed Paper for ICHEP 2004 (Beijing)

1 Introduction

This note deals with the interpretation of the results obtained by DELPHI on the searches for neutral Higgs bosons in the whole data set recorded by the experiment. The theoretical framework is the Minimal Supersymmetric Standard Model (MSSM) which, as compared with the Standard Model, has an extended Higgs sector with two doublets of Higgs fields. Two important parameters in this sector are the Higgs doublet mixing angle, α, and the ratio of the doublet vacuum expectation values, $\tan\beta$. The two-doublets of Higgs fields lead to five physical Higgs bosons, of which three are neutral. In CP-conserving MSSM models, which is the case of the scenarios considered hereafter, two of the three neutral Higgs bosons, denoted h, for the lighter one, and H, are CP-even. The third one is a CP-odd pseudo-scalar, denoted A. In e^+e^- collisions, the dominant production mechanism for the CP-even scalars is the s-channel process described in Fig. 1 which is complemented by additional t-channel diagrams in the final states where a Higgs boson is produced with neutrinos or electrons, which proceed through W^+W^- and ZZ fusions, respectively. On the other hand, the CP-odd pseudo-scalar is produced in association with either of the CP-even scalars, as depicted in Fig. 1.

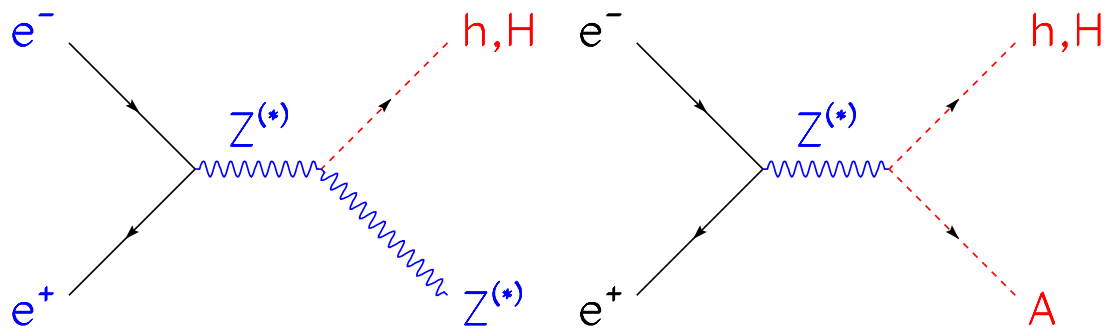

Figure 1: Main production processes of MSSM neutral Higgs bosons at LEP. Left: associated production of a Z and a CP-even Higgs boson. At LEP1, the intermediate Z is on-shell and the final Z is off-shell, while it is the reverse at LEP2. Right: pair-production of the CP-odd pseudo-scalar A and a CP-even Higgs boson. The exchanged Z is on-shell at LEP1.

In most of the MSSM parameter space, only hZ and hA productions are kinematically possible at LEP energies. These processes have complementary cross-sections since the hZZ and hAZ couplings are proportional to $\sin(\alpha-\beta)$ and $\cos(\alpha-\beta)$, respectively. If kinematically allowed, hZ production dominates at low $\tan\beta$ or at large $m_{\rm A}$, while in the rest of the parameter space, it is suppressed with respect to hA pair-production. The third neutral Higgs boson, H, in some scenarios and in limited regions of the parameter space, is light enough and can be produced with a large HZ or HA cross-section. As the HZZ (resp. HAZ) coupling is proportional to $\cos(\alpha-\beta)$ (resp. $\sin(\alpha-\beta)$), HZ production, when allowed by kinematics, arises at large $\tan\beta$, and HA production at low $\tan\beta$.

In the range of masses accessible at LEP - up to 120 (100) GeV/c^2 in $m_{\rm h}$ or $m_{\rm H}$ ($m_{\rm A}$) - and in most of the MSSM parameter space of the scenarios studied hereafter, the main decays of the three neutral Higgs bosons are into the pair of heaviest fermions

kinematically permitted. Below the $\mu^+\mu^-$ threshold, a Higgs boson would decay into $\gamma\gamma$ or e^+e^- pairs with a significant lifetime. Above the $\mu^+\mu^-$ threshold, the lifetime is negligible and Higgs bosons decay at the primary vertex. Up to 3 GeV, the main decays are into $\mu^+\mu^-$ pairs and then into hadronic channels with a large proportion of two-prong final states. Above 3 GeV, the dominant decays are successively into $c\bar{c}$, $\tau^+\tau^-$ and finally $b\bar{b}$ pairs for Higgs boson masses above 12 GeV. Besides these decays into fermions, there are also regions of the parameter space where one neutral Higgs boson can undergo cascade decays to a pair of Higgs bosons, as for example $h \to AA$. In some cases, this mode dominates over the decays into SM particles.

These different decay channels define the topologies that were searched for to cover the MSSM parameter region kinematically accessible at LEP energies. Section 2 describes these topologies as well as the definition and a summary of the techniques related to confidence levels used in the statistical interpretation of the searches. Section 3 presents the definition of the three MSSM benchmark scenarios studied in this note. Results combining LEP1 and LEP2 searches are presented in section 4 and compared with our previous results [1] which used identical experimental results but different theoretical calculations. In the present note, these have been updated to include all dominant two-loop order radiative corrections. This leads to significant changes in the Higgs boson masses and properties, and hence in the results. Another change with important consequences in the theoretical calculations is the recent update of the experimental value of the top quark mass, $m_{\rm top} = 178.0 \pm 4.3$ GeV/c^2 [2], to be compared with the previous estimate, $m_{\rm top} = 174.3 \pm 5.1$ GeV/c^2, that was used in Ref. [1]. The impact on the results of this updated measurement is discussed in section 4.

2 Experimental results and confidence levels

The different analyses performed to search for neutral Higgs bosons in the whole DELPHI data sample are summarised in Table 1 which lists the final states, mass ranges, data samples and the references for more details about the selections and their performance. This set of experimental inputs is identical to that used to derive our previous interpretation of [1]. Thus, changes in the results will reflect only the changes in the theoretical framework.

When scanning over the parameter space of a model, confidence levels are computed at each point to test the compatibility of data with the hypothesis of background only and with that of background plus signal as expected from the model. These are calculated using a modified frequentist technique based on the extended maximum likelihood ratio [19] which has also been adopted by the LEP Higgs working group. The basis of the calculation is the likelihood ratio test-statistic, $\mathcal{Q}$:

$$\ln \mathcal{Q} = -S + \sum_i \ln \frac{s_i + b_i}{b_i}$$

where the S is the total signal expected and s_i and b_i are the signal and background densities for event i. These densities are constructed using either only expected rates or also additional discriminant information, which can be one- or two-dimensional. Table 1 presents the level of discriminant information for each channel: LEP1 results are relying on rates only, while LEP2 results mix channels without or with discriminant information.

$\sqrt{s}$ (GeV)	final state	range (GeV/c^2)	$\mathcal{L}$ (pb^{-1})	disc. info.	ref.
	hZ with direct decays				
91.	$Z \to e^+e^-$, $\mu^+\mu^-$	< 0.21	2.5	no	[4]
91.	$(h \to V^0)$ $(Z \to$ any$)$	< 0.21	2.5	no	[4]
91.	$(h \to$ 2 prongs$)$ $(Z \to q\bar{q})$	$0.21 - 2.$	0.5	no	[5]
91.	$(h \to$ jet$)$ $(Z \to e^+e^-, \mu^+\mu^-)$	$1. - 20.$	0.5	no	[5]
91.	$(h \to$ jet jet$)$ $(Z \to l^+l^-, \nu\bar{\nu})$	$> 12.$	3.6	no	[6]
91.	$(h \to$ jet jet$)$ $(Z \to e^+e^-, \mu^+\mu^-, \nu\bar{\nu})$	$> 35.$	33.4	no	[7]
161.,172.	$(h \to b\bar{b})(Z \to$ any$)$, $(h \to \tau^+\tau^-)(Z \to q\bar{q})$	$> 40.$	19.9	1d	[14]
183.	$(h \to b\bar{b})(Z \to$ any$)$, $(h \to \tau^+\tau^-)(Z \to q\bar{q})$	$> 55.$	52.0	1d	[15]
189.	$(h \to b\bar{b})(Z \to$ any$)$, $(h \to \tau^+\tau^-)(Z \to q\bar{q})$	$> 65.$	158.0	2d	[16]
192.-208.	$(h \to b\bar{b})(Z \to$ any$)$	$> 12.$	452.4	2d	[17, 3]
192.-208.	$(h \to \tau^+\tau^-)(Z \to q\bar{q})$	$> 50.$	452.4	2d	[17, 3]
	hA with direct decays				
91.	4 prongs	> 0.4	5.3	no	[8]
91.	$\tau^+\tau^-$ hadrons	$> 8.$	0.5	no	[9]
91.	$\tau^+\tau^-$ jet jet	> 50	3.6	no	[10]
91.	$b\bar{b}b\bar{b}$, $b\bar{b}c\bar{c}$	$> 30.$	33.4	no	[11]
91.	$\tau^+\tau^-b\bar{b}$	$> 16.$	79.4	no	[1]
91.	$b\bar{b}b\bar{b}$	$> 24.$	79.4	no	[18]
133.	$b\bar{b}b\bar{b}$	$> 80.$	6.0	no	[13]
161.,172.	$b\bar{b}b\bar{b}$, $\tau^+\tau^-b\bar{b}$	$> 80.$	20.0	1d	[14]
183.	$b\bar{b}b\bar{b}$, $\tau^+\tau^-b\bar{b}$	$> 100.$	54.0	1d	[15]
189.	$b\bar{b}b\bar{b}$, $\tau^+\tau^-b\bar{b}$	$> 130.$	158.0	2d	[16]
192.-208.	$\tau^+\tau^-b\bar{b}$	$> 120.$	452.4	2d	[17, 3]
192.-208.	$b\bar{b}b\bar{b}$	$> 80.$	452.4	2d	[17, 3]
189.-208.	$\tau^+\tau^-\tau^+\tau^-$	$> 8.$	570.9	1d	[18]
189.-208.	$b\bar{b}b\bar{b}$	$> 24.$	610.2	no	[18]
	hZ or hA with $h \to AA$ cascade				
91.	$Z \to q\bar{q}$	< 0.21	16.2	no	[12]
91.	$(AA \to V^0V^0)$ $(Z \to$ any but $\tau^+\tau^-)$	< 0.21	9.7	no	[12]
91.	$(AA \to \gamma\gamma)$ $(Z \to$ any or $A \to \gamma\gamma)$	< 0.21	12.5	no	[12]
91.	$(AA \to$ 4 prongs$)$ $(Z \to$ any or $A \to$ 2 prongs$)$	> 0.21	12.9	no	[12]
91.	$(AA \to$ hadrons$)$ $(Z \to \nu\bar{\nu}$ or $A \to$ hadrons$)$	> 0.21	15.1	no	[12]
91.	$(AA \to \tau^+\tau^-\tau^+\tau^-)$ $(Z \to \nu\bar{\nu}$ or $A \to \tau^+\tau^-)$	> 3.5	15.1	no	[12]
161.,172.	$(AA \to$ any$)$ $(Z \to q\bar{q}, \nu\bar{\nu}$ or $A \to$ any$)$	$> 20.$	20.0	1d	[14]
183.	$(AA \to b\bar{b}b\bar{b})$ $(Z \to q\bar{q})$	$> 12.$	54.0	1d	[15]
192.-208.	$(AA \to b\bar{b}b\bar{b}, b\bar{b}c\bar{c}, c\bar{c}c\bar{c})$ $(Z \to q\bar{q})$	$> 12.$	452.4	2d	[17, 3]
192.-208.	$(AA \to c\bar{c}c\bar{c})$ $(Z \to q\bar{q})$	$> 4.$	452.4	2d	[1]

Table 1: List of signals expected from MSSM neutral Higgs bosons that were searched for in the DELPHI data sample. Indicated for each signal are the centre-of-mass energy, final-state, analysed mass range, integrated luminosity, level of discriminant information included in the confidence level estimates (none, one- or two-dimensional) and the reference where details of the analysis are published. Here h means either of the two CP-even scalars. The mass range applies to m_h for hZ production, to m_h+m_A for hA production and to m_A for $h \to AA$ processes. When no upper bound is given, the limit given by kinematics or vanishing branching fraction must be understood.

In all such channels, the first variable is the reconstructed Higgs boson mass in the hZ analyses and the sum of the reconstructed h and A masses in the hA analyses, while the second variable, if any, is channel-dependent, as specified in the references listed in the Table.

The observed value of $\mathcal{Q}$ is compared with the expected Probability Density Functions (PDFs) for $\mathcal{Q}$, which are built using Monte Carlo sampling under the assumptions that background processes only or that both signal and background are present. The confidence levels $\mathrm{CL_b}$ and $\mathrm{CL_{s+b}}$ are their integrals from $-\infty$ to the observed value of $\mathcal{Q}$. Systematic uncertainties in the rates of signal or background events are taken into account in the calculation of the PDFs for $\mathcal{Q}$ by randomly varying the expected rates while generating the distribution [20], which has the effect of broadening the expected $\mathcal{Q}$ distribution and therefore making extreme events seem more probable.

$\mathrm{CL_b}$ is the probability of obtaining a result as background-like or more so than the one observed if the background hypothesis is correct. Similarly, the confidence level for the hypothesis that both signal and background are present, $\mathrm{CL_{s+b}}$, is the probability, in this hypothesis, to obtain more background-like results than those observed. The quantity $\mathrm{CL_s}$ is defined as the ratio of these two probabilities, $\mathrm{CL_{s+b}}/\mathrm{CL_b}$. It is not a true confidence level, but a conservative pseudo-confidence level for the signal hypothesis. All exclusions discussed hereafter use $\mathrm{CL_s}$ and require it to be 5% for an exclusion confidence of 95%. As using $\mathrm{CL_s}$ instead of $\mathrm{CL_{s+b}}$ is conservative, the rate of fake exclusions is ensured to be below 5% when $\mathrm{CL_s}$ is equal to 5%.

We refer the interested reader to [1] for more details about the handling of the experimental inputs prior to the confidence level calculations. The most important issues are the estimation of expected signal and background densities from simulation, the use of a linear interpolation to estimate densities at masses, center of mass energies or $\tan\beta$ values not included in the simulation, the way non-independent channels are treated to ensure that only independent results are statistically combined, and the way the possible simultaneous production of the two CP-even scalar Higgs bosons, h and H, is accounted for.

3 The benchmark scenarios

At tree level, the production cross-sections and the Higgs branching fractions in the MSSM depend on two free parameters, $\tan\beta$ and one Higgs boson mass, or, alternatively, two Higgs boson masses, e.g. m_{A} and m_{h}. Radiative corrections introduce additional parameters related to supersymmetry breaking. Hereafter, the usual assumption that some of them are identical at a given energy scale is made: hence, the SU(2) and U(1) gaugino mass terms are assumed to be unified at the so-called GUT scale, while the sfermion mass terms or the squark trilinear couplings are assumed to be unified at the EW scale. Within these assumptions, the parameters beyond tree level are: the top quark mass, the Higgs mixing parameter, μ, the common sfermion mass term at the EW scale, M_{susy}, the SU(2) gaugino mass term at the EW scale, M_2, the gluino mass, $m_{\tilde{g}}$, and the common squark trilinear coupling at the EW scale, A. The U(1) gaugino mass term at the EW scale, M_1, is related to M_2 through the GUT relation $M_1 = (5/3)\tan^2\theta_W M_2$. The radiative corrections affect the relationships between the masses of the Higgs bosons, with the largest contributions arising from the top/stop loops. As an example, the h boson

mass, which is below that of the Z boson at tree level, increases by a few tens of GeV/c^2 in some regions of the MSSM parameter space due to radiative corrections.

3.1 The scenarios

In the following, three benchmark scenarios are considered, as suggested in Ref. [21]. These are quite representative since the limits obtained in these schemes with earlier results were only slightly reduced in more general parameter scans [17, 22]. The values of the underlying parameters in the three scenarios are quoted in Table 2.

The first two scenarios, called the $m_{\rm h}^{\rm max}$ scenario and the no-mixing scenario, differ only by the value of $X_t = A - \mu \cot \beta$, the parameter which controls the mixing in the stop sector, and hence has the largest impact on the mass of the h boson. The $m_{\rm h}^{\rm max}$ scenario leads to the maximum possible h mass as a function of $\tan \beta$. The no-mixing scenario is its counterpart with vanishing mixing, leading to upper bounds on $m_{\rm h}$ which are at least 15 GeV/c^2 lower than in the $m_{\rm h}^{\rm max}$ scheme.

The third scenario, called the large μ scenario, has a large and positive value of μ and a relatively small value of $m_{\tilde{g}}$. It predicts at least one scalar Higgs boson with a mass within kinematic reach at LEP2 in each point of the MSSM parameter space. However, there are regions for which the Higgs bosons cannot be detected because of vanishing branching fractions into b-quarks.

scenario	$m_{\rm top}$ (GeV/c^2)	$M_{\rm susy}$ (GeV/c^2)	M_2 (GeV/c^2)	$m_{\tilde{g}}$ (GeV/c^2)	μ (GeV/c^2)	X_t (GeV/c^2)
$m_{\rm h}^{\rm max}$ scenario	174.3	1000	200	800	-200	2 $M_{\rm susy}$
no-mixing	174.3	1000	200	800	-200	0
large μ	174.3	400	400	200	1000	-300

Table 2: Values of the underlying parameters for the three representative MSSM scenarios scanned in this paper. Note that X_t is $A - \mu \cot \beta$.

The values of the underlying parameters are identical to that used in our previous results [1] but the radiative corrections have been computed with all dominant two-loop order terms included, in the Feynman-diagrammatic approach [23]. In the $m_{\rm h}^{\rm max}$ and no mixing scenarios, which were already based on Feynman-diagrammatic calculations in Ref. [1] (calculations taken from Ref. [24]), the change lies in more complete two-loop order corrections. In the large μ scenario, which was relying on the renormalization group equation approach in Ref. [1] (calculations taken from Ref. [25]), the change is both in the calculation framework and in the order of the corrections.

In order to illustrate the effect of the additional correction terms, Fig. 2 and Fig. 3 compare a few properties of the Higgs bosons in the two subsequent versions of the two-loop order corrections. The models in these figures are the no mixing and $m_{\rm h}^{\rm max}$ scenarios for a top quark mass of 174.3 GeV/c^2. Fig. 2 is extracted from our previous note [1]. The figures focus on a few points that are relevant to understand the results obtained in the different scenarios. The figures about masses and cross-sections underline the importance of the signal from the heavy CP-even scalar, H, which can be kinematically accessible at LEP2 energies with a large HZ production cross-section at large $\tan \beta$ and moderate $m_{\rm A}$. The width curves demonstrate that neutral Higgs bosons can have a width exceeding

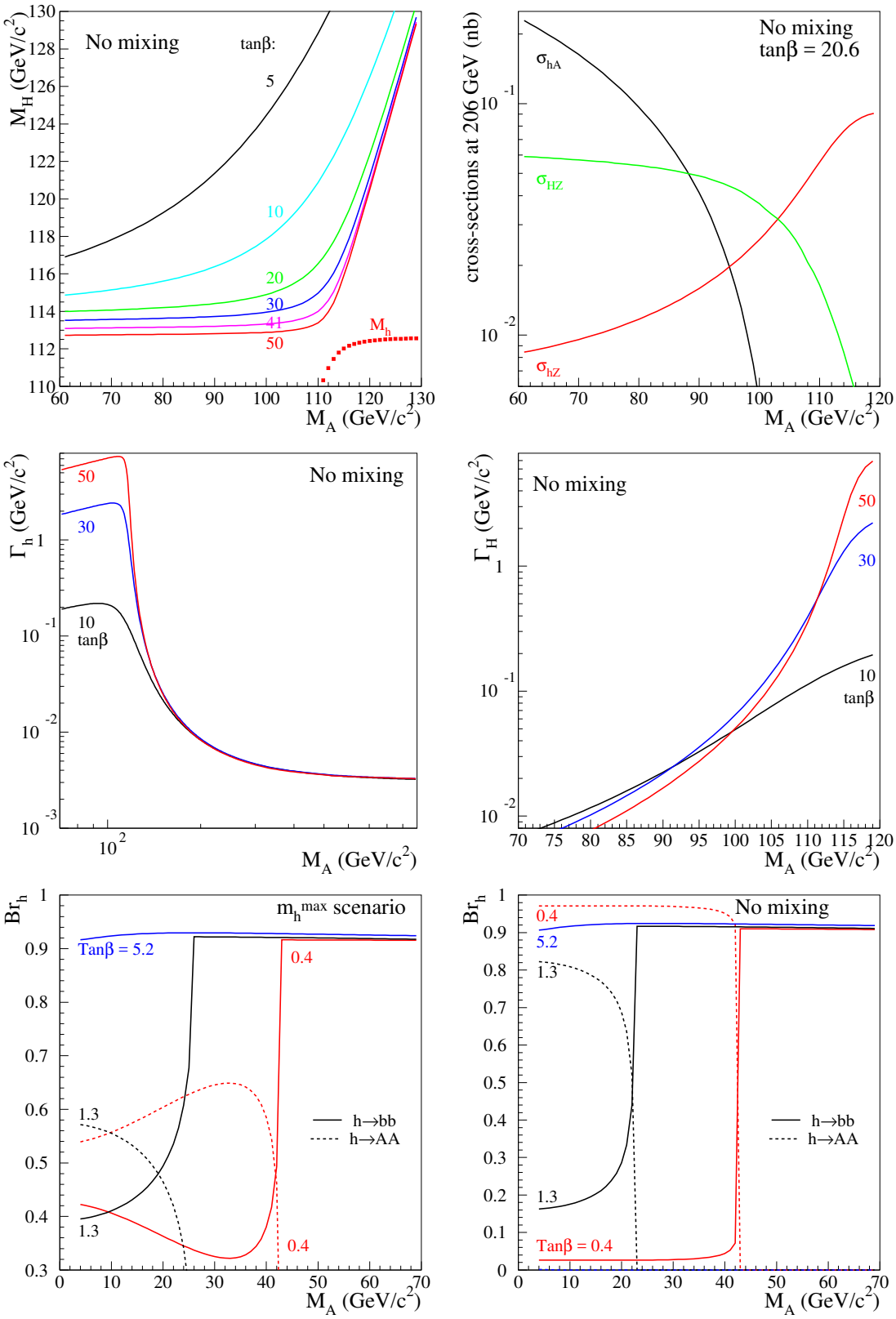

Figure 2: A few properties of the three neutral Higgs bosons of the MSSM in the no mixing and $m_{\mathrm{h}}^{\mathrm{max}}$ scenarios with $m_{\mathrm{top}} = 174.3$ GeV/c^2. Dominant two-loop order radiative corrections are partly included, as in [1]. Top: H and h masses and H, h and A production cross-sections at large $\tan\beta$. Middle: h and H width as a function of m_{A} and $\tan\beta$. Bottom: h branching fractions as a function of m_{A} at low to moderate values of $\tan\beta$. Decays into $\mathrm{b\bar{b}}$ (solid lines) and AA (dashed lines) are compared.

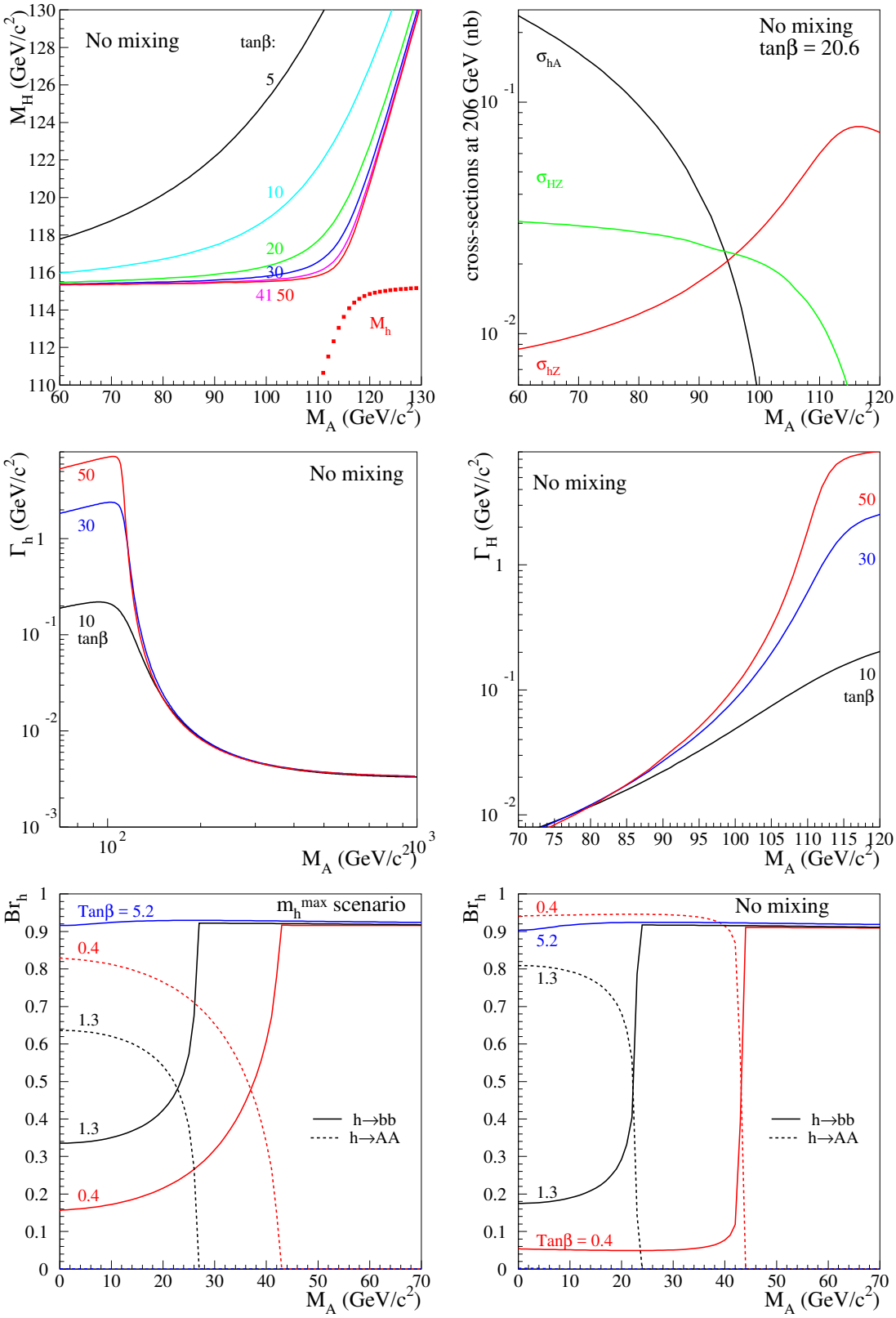

Figure 3: Same as in Fig. 2 except that all dominant two-loop order radiative corrections are included [23].

		$m_{\rm top}$ (GeV/c^2)			
scenario	rad.co.	169.2	174.3	179.4	183.0
$m_{\rm h}^{\rm max}$ scenario	old [24]	125.0	129.0	133.8	-
	new [23]	128.2	132.9	138.6	141.3
no-mixing	old [24]	111.7	114.3	116.9	-
	new [23]	112.8	115.5	118.4	-
large μ	old [25]	106.3	107.9	109.7	-
	new [23]	106.1	108.0	110.1	-

Table 3: Maximal value of $m_{\rm h}$ in the MSSM $m_{\rm h}^{\rm max}$, no mixing and large μ scenarios for two sets of radiative corrections and for a few values of $m_{\rm top}$. 183 GeV/c^2 was studied only in the MSSM $m_{\rm h}^{\rm max}$ scenario with new radiative corrections. The maximum value of $m_{\rm h}$ corresponds approximately to the minimum value of $m_{\rm H}$.

the experimental resolution at large $\tan\beta$. At moderate $m_{\rm A}$, this affects the h and A bosons and thus the hA production mode, but not the HZ one. At large $m_{\rm A}$ width effects become negligible for the h boson so that the hZ production mode, which is the only possible dominant mode in that region, is not affected. Finally, the figures about branching fractions compare the no mixing and $m_{\rm h}^{\rm max}$ scenarios at low $\tan\beta$. In the $m_{\rm h}^{\rm max}$ scenario, the h branching fraction into $\rm b\bar{b}$ always remains significant while in the no mixing scenario, it decreases at very low $\tan\beta$ at the profit of the branching fraction into AA. Comparing Fig. 2 with Fig. 3 reveals that the main effect of the more complete radiative corrections is an increase of the maximum (resp. minimum) allowed value of the h (resp. H) boson mass at fixed $\tan\beta$. As a consequence, the experimental sensitivity in $\tan\beta$ and that in $m_{\rm H}$ are expected to decrease. The cross-section curves in Fig. 2 and Fig. 3 show indeed that the HZ production cross-section drops by a factor two when improved corrections are included. On the other hand, the width effects are similar, allowing for the same treatment as in our previous interpretation [1] and the difference between the no mixing and $m_{\rm h}^{\rm max}$ scenarios at low $\tan\beta$, although reduced, remains qualitatively the same.

The impact of the new set of radiative corrections is further illustrated in Table 3 which gives the maximum value of $m_{\rm h}$ allowed by theory in the three scenarios, for the two sets of radiative corrections and for a few values of $m_{\rm top}$. The effects on the maximum value of $m_{\rm h}$ of the change in top quark mass and the improved corrections are similar and are both in the direction of an increase. They are most important in the $m_{\rm h}^{\rm max}$ scenario where they are each around 5 GeV/c^2. The effect is much smaller in the other two scenarios. It must be noted that the maximum value of $m_{\rm h}$ corresponds approximately to the minimum value of $m_{\rm H}$ in the first two scenarios, independently of $\tan\beta$, and to the minimum value of $m_{\rm H}$ allowed at large $\tan\beta$ in the large μ model.

3.2 The procedure

In the three benchmark scenarios, a scan was performed over the MSSM parameters $\tan\beta$ and $m_{\rm A}$. The range in $m_{\rm A}$ spans from 0.02 GeV/c^2, up to the maximal value allowed by each scenario [21], that is up to $M_{\rm susy}$, which is 1 TeV/c^2 in the $m_{\rm h}^{\rm max}$ and no-mixing schemes, and 400 GeV/c^2 in the large μ scenario (see Table 2). The range in

$\tan\beta$ extends from the minimal value allowed in each scenario [1] up to 50, a value chosen in the vicinity of the ratio of the top- and b-quark masses, which is an example of the large $\tan\beta$ hypothesis favoured in some constrained MSSM models [26]. The scan steps were 1 GeV/c^2 in $m_{\rm A}$ and 0.1 in $\tan\beta$ in the regions where $m_{\rm h}$ varies rapidly with these parameters. At low $m_{\rm A}$, where the decays modes change rapidly with the Higgs boson mass, values tested were 0.02, 0.1, 0.25, 0.5, 1.5 and 3 GeV/c^2.

At each point of the parameter space, the hZ and hA cross-sections and the Higgs branching fractions were taken from databases provided by the LEP Higgs working group, Ref. [27], on the basis of the theoretical calculations in Ref. [23]. The signal expectations in each channel were then derived from the theoretical cross-sections and branching fractions, the experimental luminosity and the efficiencies. If necessary, a correction was applied to account for different branching fractions of the Higgs bosons between the test point and the simulation (e.g. for the hZ process, the simulation was done in the SM framework).

For the hA channels, to account for non-negligible widths of the h and A bosons at large $\tan\beta$, efficiencies derived from simulations with h and A widths below 1 GeV/c^2 (see e.g. [3]) were applied for $\tan\beta < 30$ only. Above that value, efficiencies were linearly interpolated in $\tan\beta$ between the efficiencies from these simulations and those from simulations at $\tan\beta = 50$ where the Higgs boson widths exceed the experimental resolution (typically, 5 GeV/c^2 on the sum of the Higgs boson masses). As the Higgs boson widths grow approximately linearly with $\tan\beta$ above 30, a linear interpolation is valid. The same holds for the discriminant information, for which the same interpolation software was used for the PDF interpolation in mass or centre-of-mass energy [1]. As mentioned earlier, the hZ and HZ channels at large $\tan\beta$ are much less affected by such an effect since in most of the regions where they possibly contribute, their width is below the experimental resolution, see Fig. 3.

4 Results

The regions of the MSSM parameter space excluded at 95% CL or more by combining the results of Table 1 are discussed in turn for each scenario.

4.1 The $m_{\rm h}^{\rm max}$ scenario

The excluded regions in the ($m_{\rm h}$, $\tan\beta$), ($m_{\rm A}$, $\tan\beta$) and ($m_{\rm h}$, $m_{\rm A}$) planes are presented in Fig. 4. The inclusion of the searches for the heavy scalar, H, brings no change in the excluded regions since H is above LEP sensitivity in this scenario (see Tab. 3). Basically, the exclusion is made by the results in the hZ (hA) channels in the low (large) $\tan\beta$ region while they both contribute at intermediate values. The zoom at low $m_{\rm A}$ in the ($m_{\rm h}$, $m_{\rm A}$) projection reveals an unexcluded hole at low $m_{\rm h}$ and $\tan\beta$ above 7, thus in a region dominated by hA production. This hole is due to the lack of a search for the hA mode when $m_{\rm A}$ is below the $\mu^+\mu^-$ threshold and decays far from the primary vertex or when $m_{\rm A}$ is between the $\mu^+\mu^-$ threshold and 3 GeV/c^2 and $m_{\rm h}$ is above 10 GeV/c^2 so that a two-jet two-prong final state is to be expected. However, the limit on the Z partial width that would be due to new physics [28], $\Gamma^{\rm new} < 6.6$ MeV/c^2, translates, when

[1] The minimal value of $\tan\beta$ is 0.7 in the large μ scenario and 0.4 in the other two schemes. For lower values, some parameter combinations give rise to unphysical negative mass squared values.

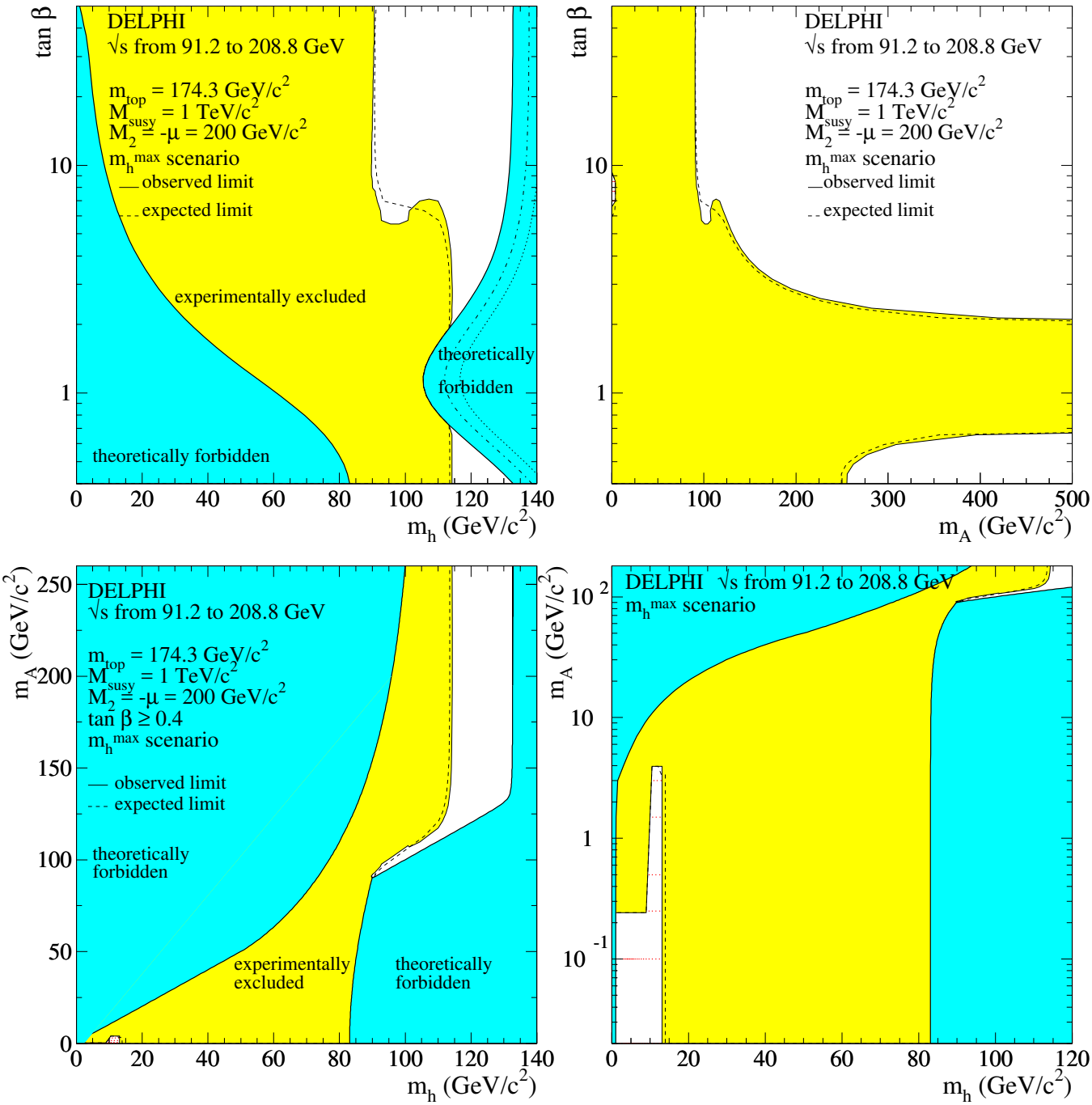

Figure 4: MSSM $m_{\mathrm{h}}^{\mathrm{max}}$ scenario: regions excluded at 95% CL by combining the results of the hZ and hA searches in the whole DELPHI data sample (light shaded area). The unexcluded region at low m_{A} is too small to be visible in the top left-hand plot. Dots indicate the additional exclusion brought by the limit on the Z partial width that would be due to new physics [28]: the unexcluded region at low m_{A} is thus fully excluded. The dashed curves show the median expected limits. The dark shaded areas are the regions not allowed by the MSSM model in this scenario. The dash-dotted (resp. dotted) line in the top left-hand plot is the theoretical upper bound for a top mass of 179.4 (resp. 183.0) GeV/c^2.

applied to the hA process, into an excluded region that encompasses the holes left by the direct searches.

Altogether, the above results thus establish the following 95% CL lower limits on $m_{\rm h}$ and $m_{\rm A}$:

$$m_{\rm h} > 89.7 \text{ GeV}/c^2 \qquad m_{\rm A} > 90.4 \text{ GeV}/c^2$$

for any value of $\tan\beta$ between 0.4 and 50. The expected median limits are 90.7 GeV/c^2 for $m_{\rm h}$ and 90.8 GeV/c^2 for $m_{\rm A}$. The observed limit in $m_{\rm A}$ ($m_{\rm h}$) is reached at $\tan\beta$ around 20 (10), in a region where both the hZ and hA processes contribute. Furthermore, there is an excluded range in $\tan\beta$ between 0.72 and 1.94 (expected [0.80-1.75]) which is valid for any value of $m_{\rm A}$ between 0.02 and 1000 GeV/c^2.

When compared to our previous results of Ref. [1], the mass limits are stable but the excluded interval in $\tan\beta$ is reduced (see Tab. 4 and 5). The reason is that the more complete radiative corrections have no impact on the value of $m_{\rm h}$ in the region of intermediate $m_{\rm A}$, where the mass limits are set. On the other hand, the excluded range in $\tan\beta$ is governed by the maximal value of $m_{\rm h}$, which is reached at large $m_{\rm A}$ where $m_{\rm h}$ is very sensitive to the additional corrections.

The $m_{\rm top}$ dependence of the above limits was also studied, as summarised in Table 5. The effect of $m_{\rm top}$ is similar to that of the new radiative corrections. The mass limits remain unchanged when varying $m_{\rm top}$, for $m_{\rm h}$ is insensitive to $m_{\rm top}$ in the region where the limits are set. On the other hand, the maximal value of $m_{\rm h}$ is very sensitive to $m_{\rm top}$, as illustrated in the top left-hand plot in Fig. 4: hence the variation of the limits in $\tan\beta$ as reported in Table 5 and Fig. 5. It must be noted that for a top mass of 183 GeV/c^2, there is no longer any exclusion in $\tan\beta$.

4.2 The no mixing scenario

The excluded regions in the ($m_{\rm h}$, $\tan\beta$), ($m_{\rm A}$, $\tan\beta$) and ($m_{\rm h}$, $m_{\rm A}$) planes are presented in Fig. 6. As pointed out in Fig. 3, in this scenario the heavy scalar, H, is kinematically accessible at large $\tan\beta$ and moderate $m_{\rm A}$, the region where the mass limits in $m_{\rm A}$ and $m_{\rm h}$ are set. Thus, allowing for its production increases the sensitivty of the searches, as shown in the top plots of Fig. 6. There are two unexcluded holes below 4 GeV/c^2 in $m_{\rm A}$. The one at low $m_{\rm h}$, similar to that encountered in the previous scenario, is excluded by the limit on $\Gamma^{\rm new}$. The second unexcluded area corresponds to $\tan\beta$ below 0.8 and $m_{\rm h}$ between 69 and 85 GeV/c^2. In that region, $m_{\rm A}$ is below the kinematic threshold $m_{\rm h} = 2m_{\rm A}$, the decay h $\rightarrow$ AA opens and supplants the h $\rightarrow$ b$\bar{\rm b}$ mode, as can be seen in Fig. 3. Our LEP2 h $\rightarrow$ AA searches having sensitivity down to the c$\bar{\rm c}$ threshold in $m_{\rm A}$ (see Table 1), the region below $m_{\rm A} = 4$ GeV/c^2 remains unexcluded. The above results thus establish the following 95% CL lower limits on $m_{\rm h}$ and $m_{\rm A}$:

$$m_{\rm h} > 90.6 \text{ GeV}/c^2 \qquad m_{\rm A} > 91.4 \text{ GeV}/c^2.$$

for any value of $\tan\beta$ between 0.8 and 50. The expected median limits are 91.1 GeV/c^2 for both $m_{\rm h}$ and $m_{\rm A}$. The observed limits in $m_{\rm A}$ and $m_{\rm h}$ are reached at $\tan\beta$ around 15, in a region where both the hZ and hA processes contribute. Furthermore, there is an excluded range in $\tan\beta$ between 0.8 and 9.36 (expected [0.88-6.97]) which is valid for any value of $m_{\rm A}$ between 0.02 and 1000 GeV/c^2.

scenario	limits	$m_{\rm top}$ (GeV/c^2) 169.2	174.3	179.4
$m_{\rm h}^{\rm max}$ scenario	$m_{\rm h}$ lower lim. (GeV/c^2)	89.7	89.7	89.7
	$m_{\rm A}$ lower lim. (GeV/c^2)	90.5	90.5	90.5
	$\tan\beta$ excluded range	0.4 - 2.87	0.54 - 2.36	0.65 - 1.94
no-mixing	$m_{\rm h}$ lower lim. (GeV/c^2)	111.7	92.0	90.2
	$m_{\rm A}$ lower lim. (GeV/c^2)	1000.	93.0	90.9
	$\tan\beta$ excluded range	0.8 - 50.	0.8 - 9.36	0.8 - 5.72

Table 4: A reminder of the 95% CL lower bounds on $m_{\rm h}$ and $m_{\rm A}$ and excluded ranges in $\tan\beta$ obtained in the MSSM $m_{\rm h}^{\rm max}$ and no mixing scenarios, as a function of $m_{\rm top}$, when dominant two-loop order radiative corrections are only partly included. This table is extracted from our previous results [1].

scenario	limits	$m_{\rm top}$ (GeV/c^2) 169.2	174.3	179.4	183.0
$m_{\rm h}^{\rm max}$ scenario	$m_{\rm h}$ lower lim. (GeV/c^2)	89.7	89.7	89.7	89.7
	$m_{\rm A}$ lower lim. (GeV/c^2)	90.4	90.4	90.4	90.4
	$\tan\beta$ excluded range	0.59 - 2.36	0.72 - 1.94	0.97 - 1.44	none
no-mixing	$m_{\rm h}$ lower lim. (GeV/c^2)	112.8	90.6	90.0	
	$m_{\rm A}$ lower lim. (GeV/c^2)	1000.	91.4	90.6	
	$\tan\beta$ excluded range	0.8 - 50.	0.8 - 9.36	0.8 - 5.30	

Table 5: Updated 95% CL lower bounds on $m_{\rm h}$ and $m_{\rm A}$ and excluded ranges in $\tan\beta$ obtained in the MSSM $m_{\rm h}^{\rm max}$ and no mixing scenarios, as a function of $m_{\rm top}$, when dominant two-loop order radiative corrections are fully included.

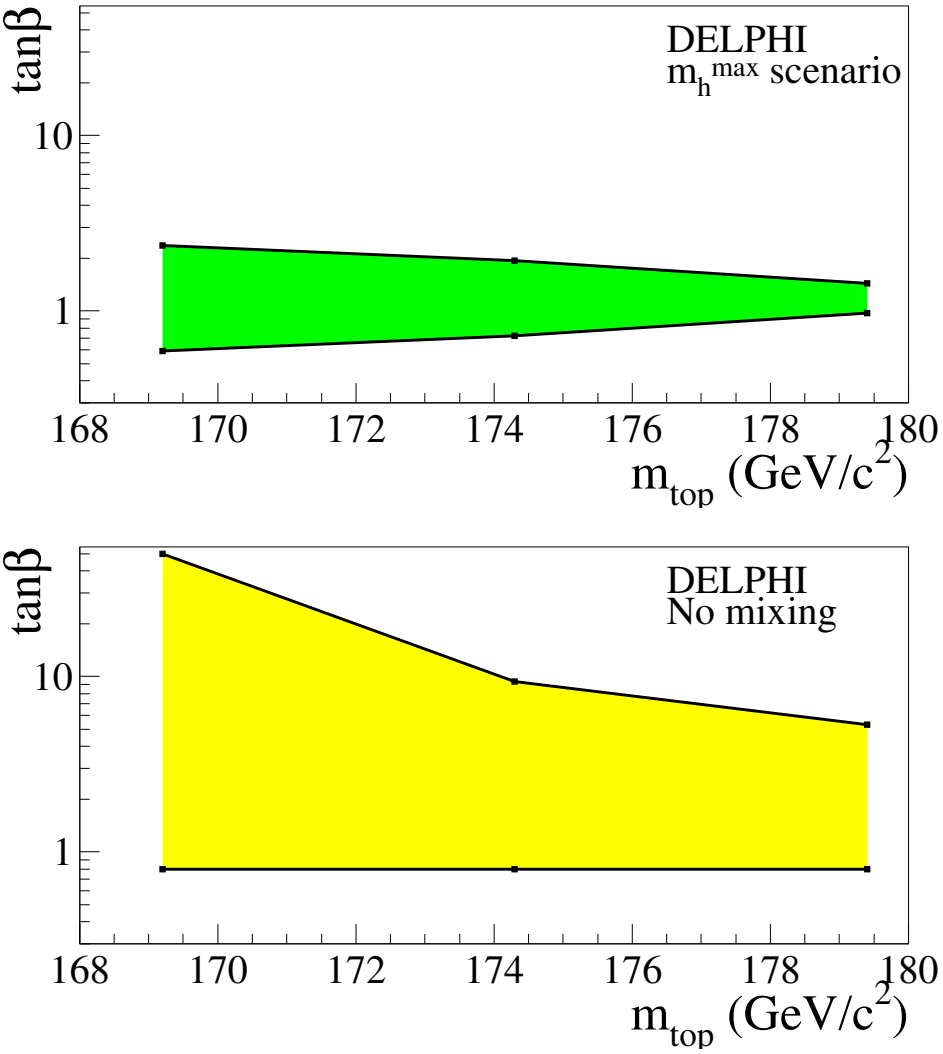

Figure 5: $m_{\rm top}$ dependence of the ranges in $\tan\beta$ excluded at 95% CL in the $m_{\rm h}^{\rm max}$ scenario (top) and in the no mixing scenario (bottom).

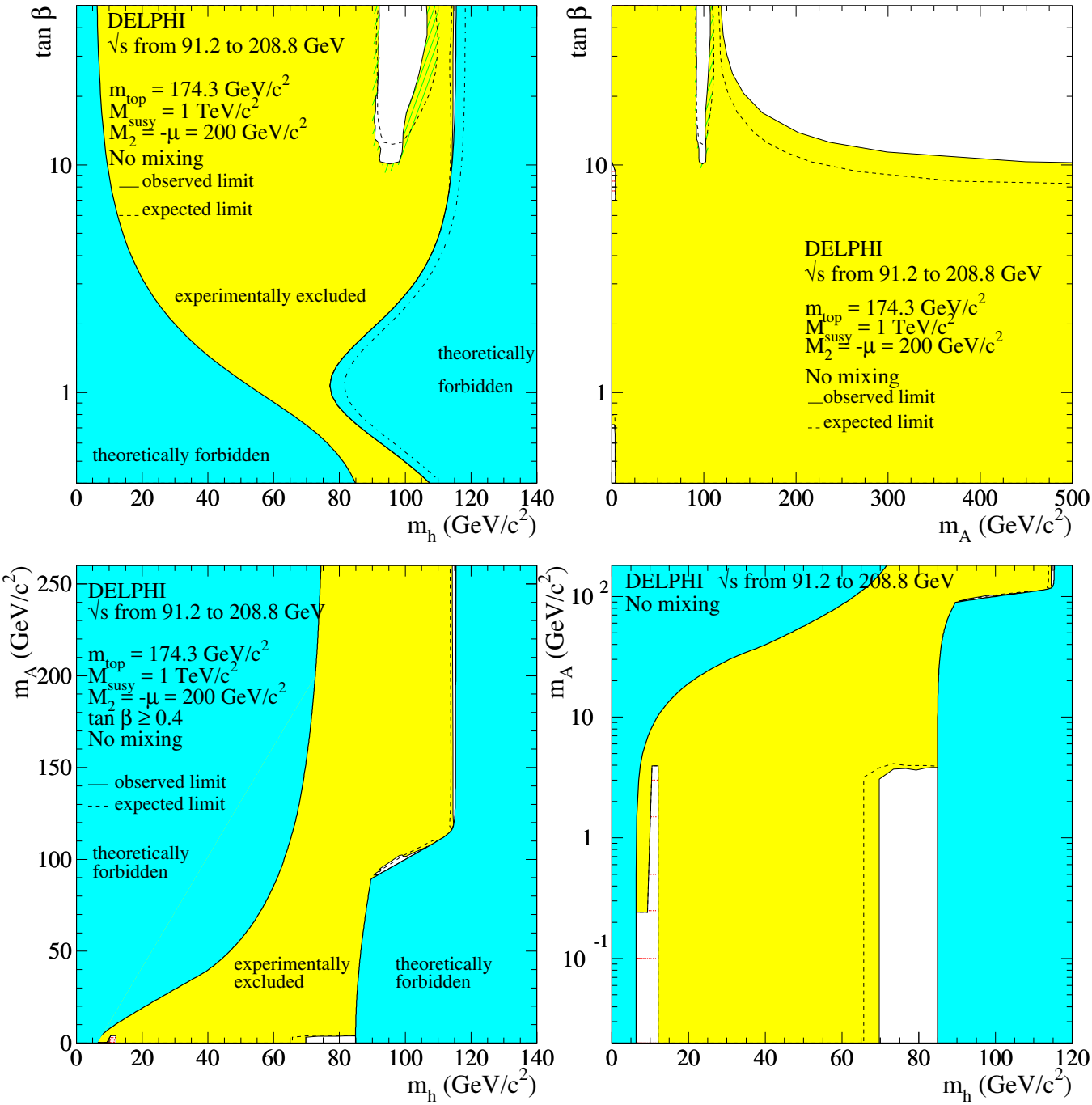

Figure 6: MSSM no-mixing scenario: regions excluded at 95% CL by combining the results of the h, A and H searches in the whole DELPHI data sample (light shaded and hatched areas). The hatched area in the top plots is that excluded by the searches for the heavy scalar Higgs boson, H. There are unexcluded regions at low m_{A} which are too small to be visible in the top left-hand plot. Dots indicate the additional exclusion from the limit on the Z partial width that would be due to new physics [28]: the unexcluded region at low m_{A} and m_{h} is thus fully excluded. The dashed curves show the median expected limits. The dark shaded areas are the regions not allowed by the MSSM model in this scenario. The dash-dotted line in the top left-hand plot is the theoretical upper bound for a top mass of 179.4 GeV/c^2.

When compared to our previous results of Ref. [1], the mass limits are reduced but the excluded interval in $\tan\beta$ is stable (see Tab. 4 and 5). The reason for the decrease of the mass limits is that the more complete radiative corrections lead to an increase of the value of $m_{\rm H}$ in the region of intermediate $m_{\rm A}$ and large $\tan\beta$ (see Figs. 2 and 3), which translates into a loss of sensitivity in this region where the mass limits are set. On the other hand, the maximal value of $m_{\rm h}$, which governs the exclusion in $\tan\beta$, is weakly affected by the additional corrections (see Tab. 3) and so is the excluded range in $\tan\beta$.

The $m_{\rm top}$ dependence of the above limits was studied, as shown in Table 5 and Fig. 5. In this scenario, both the mass limits and the excluded range in $\tan\beta$ change when varying $m_{\rm top}$. Indeed, as already mentioned, the mass limits in $m_{\rm A}$ and $m_{\rm h}$ rely on the searches for H, whose mass is very sensitive to $m_{\rm top}$ in the region where the limits are set. Similarily, the maximal value of $m_{\rm h}$, which governs the limits in $\tan\beta$, is reached at large $m_{\rm A}$ where $m_{\rm h}$ is very sensitive to $m_{\rm top}$ (see Tab. 3). Note that for a top mass of 169 GeV/c^2, $m_{\rm H}$ decreases by 3 GeV/c^2 in the region where the mass limits are set, making the H signal more within the sensitivity of LEP2: the large $\tan\beta$ region of the no mixing scenario is then fully accessible and found to be excluded.

4.3 The large μ scenario

The excluded regions in the large μ scenario are presented in the ($m_{\rm h}$, $\tan\beta$) and ($m_{\rm A}$, $\tan\beta$) planes in Fig. 7, for two values of the top quark mass, namely 174.3 and 179.4 GeV/c^2. A large fraction of the allowed domain is excluded by the searches for the h, A and H Higgs bosons. In particular, given that the theoretical upper bound on the h boson mass in that scenario is low (around 110.0 GeV/c^2, see Tab. 3), the sensitivity of the hZ channels is high even at large $\tan\beta$, which explains why the excluded region reaches the theoretically forbidden area for large values of $\tan\beta$. Moreover, the value of the upper bound on $m_{\rm h}$ is also the theoretical lower bound on $m_{\rm H}$ at large $\tan\beta$, which explains why allowing for the production of H translates into a significant gain in exclusion.

There are however several unexcluded holes. At low $m_{\rm A}$ and $\tan\beta$ above 1, these are due to the lack of searches for the topology with two jets and hadrons as expected from the hA process with one Higgs boson of mass above the $\rm b\bar{b}$ threshold and the other one with a mass between 1 and 4 GeV/c^2. These points are all excluded by the limit on $\Gamma^{\rm new}$. At low $m_{\rm A}$ and $\tan\beta$ below 1, the hole observed for a top quark mass of 179.4 GeV/c^2 corresponds to large hZ and HA production cross-sections, but h, although above the $\rm b\bar{b}$ threshold is decoupled from $\rm b\bar{b}$, while H and A are in the same mass range as above, that is with no corresponding experimental search. Note that for a top quark mass of 174.3 GeV/c^2, the h branching fraction into $\rm b\bar{b}$ is a bit increased, leading to the exclusion of the hole. There is another larger unexcluded region at higher masses and $\tan\beta$ above 10. At moderate $m_{\rm A}$ (around 100 GeV/c^2), hZ and hA productions are low due to weak hZZ couplings for hZ and to kinematics for hA. On the other hand, HZ production is large but H is decoupled from $\rm b\bar{b}$. At larger $m_{\rm A}$, hA and HZ productions are kinematically forbidden, hZ production is large but the h$\rightarrow\rm b\bar{b}$ branching fraction vanishes. In this area, the Higgs boson whose production is allowed (H or h) has a large branching fraction into hadrons. Testing these points with the results from the searches for hadronic decays of Higgs bosons produced in the hZ or HZ modes will be dealt with in a forthcoming paper.

Finally, when compared to our previous results [1], the non-excluded region is slightly larger and modified, due to the additional corrections and the new theoretical calculation

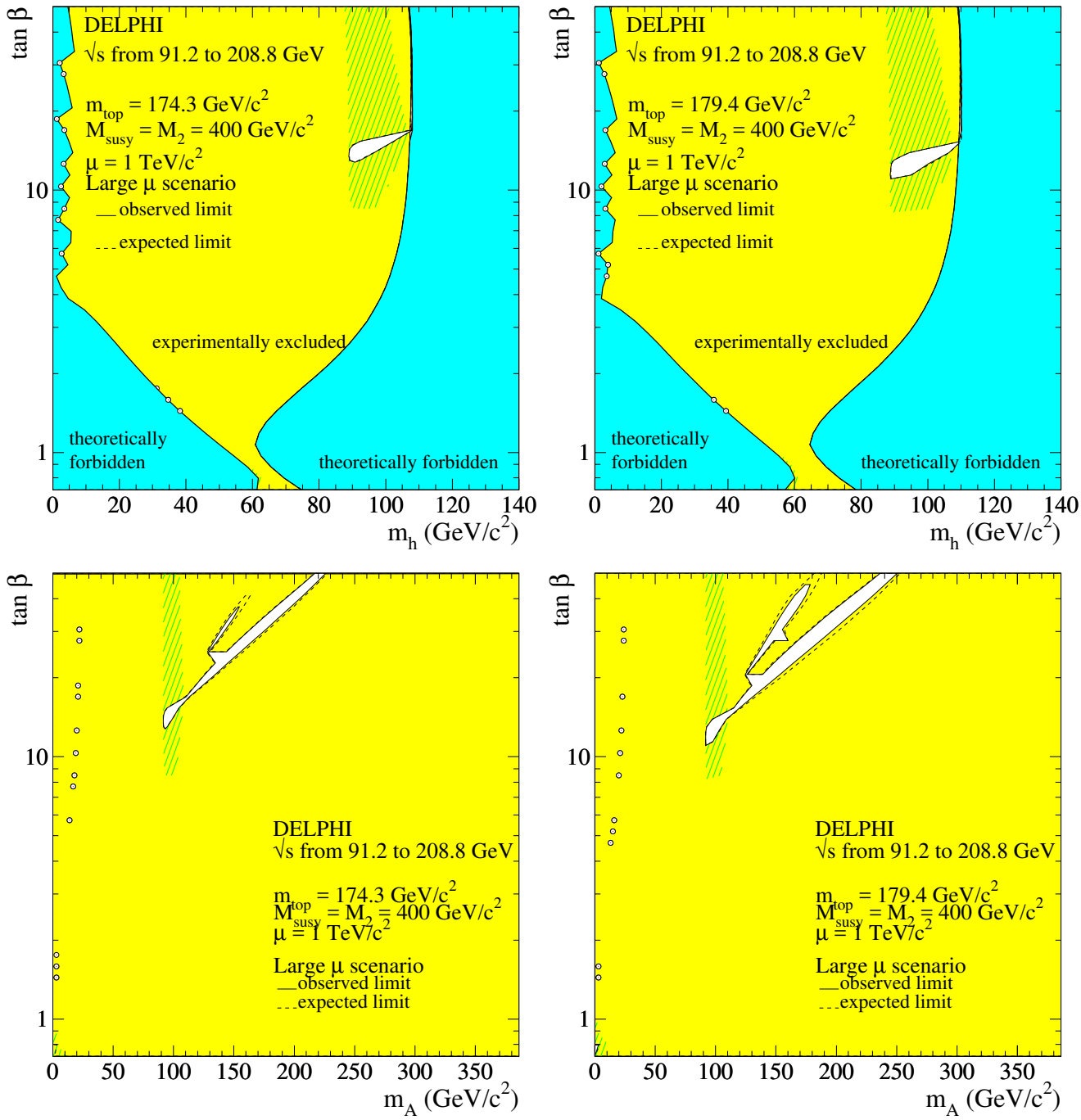

Figure 7: MSSM large μ scenario: regions excluded at 95% CL by combining the results of the h, A and H searches in the whole DELPHI data sample (light shaded and hatched areas). Results are shown for two values of the top mass, 174.3 and 179.4 GeV/c^2. The hatched areas are excluded when the searches for the heavy scalar Higgs boson, H, are taking into account. The unexcluded regions at low m_A and tan β above 1 are all excluded by the limit on the Z partial width that would be due to new physics [28]. The dashed curves show the median expected limits. The dark shaded areas are the regions not allowed by the MSSM model in this scenario.

framework. Similarily, increasing the top quark mass from 174.3 to 179.4 GeV/c^2 leads to a larger unexcluded area, for there are more points with vanishing h or H branching fractions into $b\bar{b}$.

5 Conclusions

Combining the results of the searches for the three MSSM neutral Higgs bosons performed in the whole data sample of the DELPHI experiment establishes the following limits at 95% of CL in the framework of the m_h^{max} scenario with $m_{top} = 174.3$ GeV/c^2:

$m_h > 89.7$ GeV/c^2	and	$m_A > 90.4$ GeV/c^2	for any $\tan\beta$ between 0.4 and 50,
$\tan\beta < 0.72$	or	$\tan\beta > 1.94$	for any m_A between 0.02 and 1000 GeV/c^2.

The mass limits are insensitive to variations of the top quark mass in the range between 169.2 and 183.0 GeV/c^2. The excluded range in $\tan\beta$ decreases with increasing m_{top}. As an example, with $m_{top} = 179.4$ GeV/c^2, the upper and lower bounds on $\tan\beta$ becomes 0.97 and 1.44, respectively, and no bound can be set on $\tan\beta$ at $m_{top} = 183.0$ GeV/c^2.

In the no mixing scenario with $m_{top} = 174.3$ GeV/c^2, the limits are:

$m_h > 90.6$ GeV/c^2	and	$m_A > 91.4$ GeV/c^2	for any $\tan\beta$ between 0.8 and 50,
$\tan\beta < 0.80$	or	$\tan\beta > 9.36$	for any m_A between 0.02 and 1000 GeV/c^2.

The higher mass limits in the no mixing scenario come from the signal from the heavy CP-even scalar, H, which, in that scenario, is within the sensitivty of LEP2 in the region of the MSSM parameter space where the mass limits are set. Both the mass and $\tan\beta$ limits are sensitive to the value of the top quark mass. As an example, with $m_{top} = 179.4$ GeV/c^2, the lower bounds on m_h and m_A becomes 90.0 and 90.6 GeV/c^2, respectively, and the upper and lower bounds on $\tan\beta$ becomes 0.80 and 5.30, respectively.

Finally, the same results, when applied to the large μ scenario allow to exclude a large fraction of the parameter space. In particular, including the production of the CP-even scalar translates into a significant gain in exclusion in this scenario. The non-excluded regions are due to vanishing h or H branching fractions into $b\bar{b}$. The exclusion contour has a moderate dependence on the top quark mass value.

References

[1] DELPHI 2003-045-CONF-665, *DELPHI results on neutral Higgs bosons in MSSM benchmark scenarios*, contribution to the 2003 summer conferences.

[2] CDF and D0 collaborations and the Tevatron electroweak working group, *Combination of CDF and D0 results on the top-quark mass*, hep-ex/0404010.

[3] DELPHI Collaboration, J. Abdallah et al., Eur. Phys. J. **C32** (2004) 145.

[4] DELPHI Collaboration, P. Abreu et al., Z. Phys. **C51** (1991) 25

[5] DELPHI Collaboration, P. Abreu et al., Nucl. Phys. **B342** (1990) 1

[6] DELPHI Collaboration, P. Abreu et al., Nucl. Phys. **B373** (1992) 3

[7] DELPHI Collaboration, P. Abreu et al., Nucl. Phys. **B421** (1994) 3.

[8] S.Dagoret, PhD thesis, Université de Paris-Sud, centre d'Orsay, LAL-preprint 91-12 (may 1991).

[9] DELPHI Collaboration, P. Abreu et al., Phys. Lett. **B245** (1990) 276.

[10] DELPHI Collaboration, P. Abreu et al., Nucl. Phys. **B373** (1992) 3.

[11] DELPHI Collaboration, P. Abreu et al., Z. Phys. **C67** (1995) 69.

[12] DELPHI 92-80 Dallas PHYS 191, *Neutral Higgs Bosons in a Two Doublet Model*, contribution to the 1992 ICHEP conference; quoted by G.Wormser, in proc. of the XXVI ICHEP conference (Dallas, August 1992), Vol. 2, pages 1309-14, ref. 4.

[13] DELPHI Collaboration, P. Abreu et al., Z. Phys. **C73** (1996) 1.

[14] DELPHI Collaboration, P. Abreu et al., Eur. Phys. J. **C2** (1998) 1.

[15] DELPHI Collaboration, P. Abreu et al., Eur. Phys. J. **C10** (1999) 563.

[16] DELPHI Collaboration, P. Abreu et al., Eur. Phys. J. **C17** (2000) 187, addendum Eur. Phys. J. **C17** (2000) 529.

[17] DELPHI Collaboration, J. Abdallah et al., Eur. Phys. J. **C23** (2002) 409.

[18] DELPHI Collaboration, J. Abdallah et al., CERN-EP/2003-061, submitted to E. Phys. J.

[19] A.L. Read, *Modified Frequentist Analysis of Search Results (The CL_s Method)*, in CERN Report 2000-005, p. 81 (2000), edited by F.James, L.Lyons and Y.Perrin.

[20] R.D. Cousins and V.L. Highland, Nucl. Instr. and Meth. **A320** (1992) 331.

[21] M. Carena, S. Heinemeyer, C. Wagner and G. Weiglein, *Suggestions for improved benchmark scenarios for Higgs boson searches at LEP2* CERN-TH/99-374, DESY 99-186 or hep-ph/9912223;
M. Carena, S. Heinemeyer, C. Wagner and G. Weiglein, Eur. Phys. J. **C26** (2003) 601.

[22] DELPHI 2003-039-CONF-659, *Complete DELPHI data: Limits on Higgs Boson Masses and tanβ from a MSSM Parameter Scan*, contribution to the 2003 summer conferences.

[23] G. Degrassi, S. Heinemeyer, W. Hollik, P. Slavich and G. Weiglein, Eur. Phys. J. **C28** (2003) 133.

[24] S. Heinemeyer, W. Hollik and G. Weiglein, Eur. Phys. J. **C9** (1999) 343.

[25] M. Carena, M. Quiros and C.E.M. Wagner, Nucl. Phys. **B461** (1996) 407
M. Carena, M. Quiros and C.E.M. Wagner, Phys. Rev. **D62** (2000) 055008.

[26] M. Carena, S. Pokorski and C.E.M. Wagner, Nucl. Phys. **B406** (1993) 59.

[27] ALEPH, DELPHI, L3, OPAL Collaborations and the LEP Higgs working group, *Search for neutral MSSM Higgs bosons at LEP*, contribution to the 2004 summer conferences.

[28] DELPHI Collaboration, P. Abreu et al., Eur. Phys. J. **C16** (2000) 371.